

# ADVANCED MATERIALS

**Supporting Information**

for

*Advanced Materials*, adma.200602934

© Wiley-VCH 2007  
69451 Weinheim, Germany

## Supporting Information to

### Nano-Decoding by Dewetting

By G. G. Baralia, C. Filiâtre, B. Nysten, and A. M. Jonas

### Estimation of the surface tension of the substrates by van Oss-Chaudhury-Good and Owens-Wendt methods

Two methods, independently or jointly, were used to estimate the surface free energy components of our surfaces: the van Oss-Chaudhury-Good<sup>[1]</sup> (OCG) and Owens-Wendt methods,<sup>[2]</sup> which respectively rely on the following equations:

$$\gamma_l(1 + \cos \theta) = 2 \left( \sqrt{\gamma_s^d \gamma_l^d} + \sqrt{\gamma_l^+ \gamma_s^-} + \sqrt{\gamma_l^- \gamma_s^+} \right) \quad (1)$$

$$\gamma_l(1 + \cos \theta) = 2\sqrt{\gamma_s^d \gamma_l^d} + 2\sqrt{\gamma_s^p \gamma_l^p} \quad (2)$$

In (1) and (2),  $\theta$  is the value of the contact angle of a liquid on the solid substrate,  $\gamma$ ,  $\gamma^d$ ,  $\gamma^p$ ,  $\gamma^+$ ,  $\gamma^-$  are the total, dispersive, polar, acid (electron-acceptor) and base (electron-donor) components of the surface free energy of the liquid respectively, and  $\gamma_s^d$ ,  $\gamma_s^p$ ,  $\gamma_s^+$ ,  $\gamma_s^-$  are the dispersive, polar, acid and base components of the surface free energy of the substrate, respectively. Table S1 summarizes the values of the contact angles of different liquids on films of PS ( $M_n = 66,300$  g/mol,  $M_w = 67,626$  g/mol, from Polymer Laboratories) and of PEO ( $M_w \sim 100,000$  g/mol, from Aldrich) spin-coated on Si, on perfluorinated and amine-ended silane monolayers on Si, and on thermal  $\text{SiO}_2$ . The van Oss-Chaudhury-Good method was used to determine the surface free energy components for the two silanized substrates as well as for the  $\text{SiO}_2$  substrate. A set of three equations, in terms of measured contact angles of two polar liquids (see Table S1) and one apolar liquid (diiodomethane) on the same solid, was solved for  $\gamma_s^d$ ,  $\gamma_s^+$  and  $\gamma_s^-$  (where the parameters for the liquids:  $\gamma_i^d$ ,  $\gamma_i^+$ ,  $\gamma_i^-$ ,  $i = 1, 2$  or 3 are known, and were taken as given in<sup>[3]</sup>). For the polymers, the two methods were used jointly.

First, a graph of  $\frac{\gamma_l(1 + \cos \theta)}{2\sqrt{\gamma_l^d}} = f \left( \frac{\sqrt{\gamma_l^p}}{\sqrt{\gamma_l^d}} \right)$  was plotted after measuring the contact angle  $\theta$  of various liquids (having both dispersive and polar components in their surface tensions) against the substrates. The line passing through the data intercepts the vertical axis at  $\sqrt{\gamma_s^d}$ , whereas its slope is  $\sqrt{\gamma_s^p}$  (Figure S1).

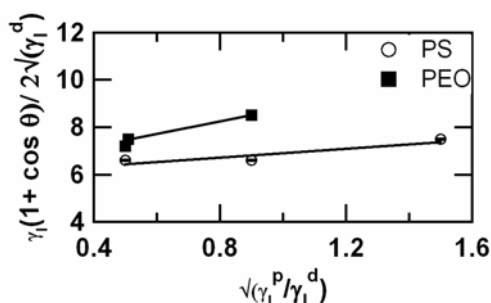


**Figure S1**  $\frac{\gamma_l(1 + \cos \theta)}{2\sqrt{\gamma_l^d}} = f \left( \frac{\sqrt{\gamma_l^p}}{\sqrt{\gamma_l^d}} \right)$  plot used to approximate the dispersive and polar free energies of the PS and PEO substrates (see Table S2).

The data were fitted to linear relationships, taking into account error bars on  $\frac{\gamma_l(1 + \cos \theta)}{2\sqrt{\gamma_l^d}}$

computed from the errors associated to the measurement of contact angles (reported in Table S1). Standard errors on the fitted parameters were estimated from the diagonal components of the covariance matrix associated with the fits.<sup>[4]</sup> Second, a set of two equations, in terms of measured contact angles of two polar liquids on the same solid, was solved for  $\gamma_s^+$  and  $\gamma_s^-$  (where the parameters for the liquids:  $\gamma_i^+$ ,  $\gamma_i^-$ ,  $i = 1$  or 2 are known from<sup>[3]</sup> and the values of the dispersive components of the surface tension of the polymers ( $\gamma_s^d$ ) were taken as given in<sup>[5]</sup>). Table S2 gives the values of the dispersive, polar, acid and base components of the surface tension of the substrates.

**Table S1** Average contact angle values (3 drops) of various liquids on PS or PEO films spin-coated on Si, on perfluorinated or amine-ended silane monolayers on Si and on 600 nm thick thermally grown SiO<sub>2</sub>

Substrate	DMSO(°)*	Water(°)	Glycerol(°)	Diiodomethane(°)
PS	37.4±0.8	92.3±0.2	-	-
PEO	16.3±0.2	Film dissolution	57.3±0.2	-
Silane -CF <sub>3</sub>	92.3±1.3	110.4±0.2	-	87.9±1.0
Silane -NH <sub>2</sub>	-	56.8±1.0	49.0±0.3	38.8±0.1
“piranha”-cleaned thermal SiO <sub>2</sub> (600 nm)	-	21.2±0.4	10.3±0.3	28.9±0.4

\*Dimethyl sulfoxide (DMSO).

The interfacial energy between two materials 1 and 2 can be determined from the following relation:

$$\gamma_{12} = \gamma_{12}^d + \gamma_{12}^p \quad (3)$$

where  $\gamma_{12}^d$  and  $\gamma_{12}^p$  are the dispersive and polar interfacial energies between the two materials, 1 and 2, and have the following expressions:<sup>[1],[6],[7]</sup>

$$\gamma_{12}^d = \gamma_1^d + \gamma_2^d - 2\sqrt{\gamma_1^d \gamma_2^d} \quad (4)$$

$$\gamma_{12}^p = 2\left(\sqrt{\gamma_1^+} - \sqrt{\gamma_2^+}\right)\left(\sqrt{\gamma_1^-} - \sqrt{\gamma_2^-}\right) \quad (5)$$

where  $\gamma_i^d$ ,  $\gamma_i^+$ ,  $\gamma_i^-$  ( $i = 1$  or 2) are the dispersive, acid and base components of the surface tension of the two materials.

**Table S2** Components of the surfaces tension determined by Owens-Wendt and van Oss-Chaudhury-Good methods

Substrate	$\gamma^d$ (mJ/m <sup>2</sup> )	$\gamma^+$ (acid, mJ/m <sup>2</sup> )	$\gamma^-$ (base, mJ/m <sup>2</sup> )	$\gamma^p$ (mJ/m <sup>2</sup> ) <sup>a</sup>	$\gamma^p$ (mJ/m <sup>2</sup> ) <sup>c</sup>
PS	33.9*	35.8±0.5 <sup>a</sup>	0.5±0.1 <sup>d</sup>	0.7±0.01 <sup>d</sup>	1.2±0.1
PEO	30.7*	37.8±0.2 <sup>a</sup>	1.7±0.01 <sup>d</sup>	13.4±0.5 <sup>d</sup>	9.4±0.2
Silane-CF <sub>3</sub>	13.7±0.5 <sup>b</sup>	16.8±0.4 <sup>a</sup>	0.2±0.1 <sup>b</sup>	0.8±0.2 <sup>b</sup>	0.7±0.1
Silane-NH <sub>2</sub>	40.2±0.03 <sup>b</sup>	39.7±0.03 <sup>a</sup>	1.0±0.03 <sup>b</sup>	18.5±1.1 <sup>b</sup>	8.6±0.1
“piranha”-cleaned Thermal SiO <sub>2</sub> (600 nm)	44.7±0.2 <sup>b</sup>	43.2±0.2 <sup>a</sup>	2.7±0.1 <sup>b</sup>	37.3±0.7 <sup>b</sup>	24.4±0.1

\*Values reported elsewhere.<sup>[5]</sup> <sup>a</sup>Values determined by the Owens-Wendt method.<sup>[2]</sup> <sup>b</sup>Values determined by the OCG method.<sup>[1]</sup> <sup>c</sup>Values determined using  $\gamma_p = 2\sqrt{\gamma^+ \gamma^-}$ .<sup>[7]</sup> <sup>d</sup>Values determined by the OCG method,<sup>[1]</sup> using  $\gamma_{PS}^d = 33.9$  mJ/m<sup>2</sup> and  $\gamma_{PEO}^d = 30.7$  mJ/m<sup>2</sup>.

For the poly(styrene-ethylene oxide) block copolymer, the interfacial energy between the polystyrene and polyethylene oxide blocks is essentially of polar nature:

$$\gamma_{S-EO} = 2\left(\sqrt{\gamma_S^+} - \sqrt{\gamma_{EO}^+}\right)\left(\sqrt{\gamma_S^-} - \sqrt{\gamma_{EO}^-}\right) + \gamma_S^d + \gamma_{EO}^d - 2\sqrt{\gamma_S^d \gamma_{EO}^d} \quad (6)$$

$= 3.4^{(p)} + 0.1^{(d)} = 3.5 \text{ mJ/m}^2$ ,  
using the values mentioned in Table S2.

**Table S3** Interfacial tensions between two different materials (1 and 2)

Materials (1-2)	$\gamma_{1-2}$ (mJ/m <sup>2</sup> )
PS-PEO	3.5±0.2
PS-NH <sub>2</sub>	2.4±0.2
PEO-NH <sub>2</sub>	0.2±0.3
PSPEO-NH <sub>2</sub>	0.5±0.04
PSPEO-CF <sub>3</sub>	6.1±0.9

Table S3 gives the interfacial tensions between the two polymer blocks as well as between the block copolymer and the blocks and an amine-ended silane substrate.

For PS-PEO thin film, a simple criterion predicts a surface-induced transition, from hexagonally packed cylinders to a lamellar phase<sup>[6],[8]</sup> since

$$\Delta\gamma = \gamma_{\text{PS}} - \gamma_{\text{PEO}} = 8.1 \text{ mJ/m}^2 > \gamma_{\text{S-EO}} = 3.5 \text{ mJ/m}^2.$$

## Theoretical predictions regarding the stability of the PS-PEO film on silanized thermal SiO<sub>2</sub>

From the sign of the spreading coefficient ( $S$ ) and of the Hamaker constant of the system SiO<sub>2</sub>-PSPEO-air ( $A_{\text{SiO}_2\text{-PSPEO-air}}$ ), the stability of the block copolymer on the considered substrates can be predicted (Table S4). Unstability of the film require  $A > 0$ , whereas if  $A < 0$  the film will be stable for  $S > 0$  and metastable if  $S < 0$ .

The Hamaker constant was computed as:

$$A_{\text{SiO}_2\text{-PSPEO-air}} = \sqrt{A_{\text{PSPEO}}} \left( \sqrt{A_{\text{PSPEO}}} - \sqrt{A_{\text{SiO}_2}} \right) \quad (7)$$

where  $A_{\text{SiO}_2} \cong 6.5 \cdot 10^{-20} \text{ J}^{[9]}$  and  $A_{\text{PSPEO}} \cong 0.35 A_{\text{PEO}} + 0.65 A_{\text{PS}}$ , with  $A_{\text{PEO}}$  and  $A_{\text{PS}}$  the Hamaker constants of PEO and PS, respectively. For both polymers, the Hamaker constant was approximated as:

$$A_i = 24\pi d_0^2 \gamma_i^d, \quad i = \text{PS or PEO},$$

where  $d_0$  is the average interfacial distance, typically taken as  $1.58 \pm 0.08 \text{ \AA}$ .<sup>[1]</sup> Note that the presence of the silane monolayer was neglected for this computation, a valid approximation since the copolymer film is much thicker than the silane monolayers.<sup>[10]</sup> The Hamaker constant is reported in Table S4. Depending of the value selected for  $\gamma_{\text{PS}}^d$  and  $\gamma_{\text{PEO}}^d$  (Table S2),  $A_{\text{SiO}_2\text{-PSPEO-air}}$  is found to be positive or negative. This is because the Hamaker constants of polymers and SiO<sub>2</sub> are close, which results in a low precision on  $A_{\text{SiO}_2\text{-PSPEO-air}}$ , as shown by equation (7). However, the experiments reported in the paper and summarized in Figure S1 of the paper clearly indicate that the film dewets by nucleation and growth of holes, which practically rules out unstability of the film.

The spreading coefficient of the copolymer on silane monolayers was computed as:

$$S = \gamma_{\text{silane}} - \gamma_{\text{PSPEO}} - \gamma_{\text{PSPEO/silane}},$$

where  $\gamma_{\text{PSPEO}} = 39.5 \pm 0.3 \text{ mJ/m}^2$ . Here again, the close proximity of  $\gamma_{\text{silane-NH}_2}$  and  $(\gamma_{\text{PSPEO}} + \gamma_{\text{PSPEO/silane}})$  results in a large relative error on  $S_{\text{PSPEO/silane-NH}_2}$ , whose sign cannot be decided unambiguously. However, the experimental observed dewetting of PSPEO on the NH<sub>2</sub>-ended silane monolayer testifies for the metastable character of the film. By contrast, the very low surface tension of the perfluorinated silane monolayer allows us to predict that  $S_{\text{PSPEO/silane-CF}_3} < 0$ , which is compatible with the experimental observations.

**Table S4** Theoretical prediction regarding the stability of the PSPEO on the silanized SiO<sub>2</sub>

(PSPEO on) Substrate	Spreading coefficient (S) (mJ/m <sup>2</sup> )	Hamaker constant $A_{\text{SiO}_2\text{-PSPEO-air}}$ (J)
SiO <sub>2</sub> -NH <sub>2</sub>	0.2 ± 0.3 or -0.3 ± 0.3	-1.7 × 10 <sup>-21</sup> or
SiO <sub>2</sub> -CF <sub>3</sub>	-28.8 ± 1 or -31.9 ± 1	1.8 × 10 <sup>-21</sup>

## Structural data on dewetted films

On the homogeneous amine-ended substrates, X-ray reflectivity (XRR) spectra and AFM phase images, before and after the dewetting process, showed essentially dry regions between the droplets (Figures S2 and S3).

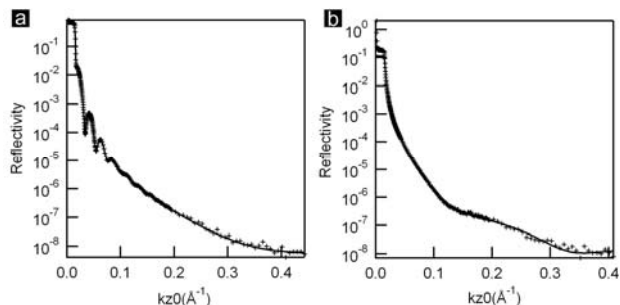


**Figure S2** X-ray reflectivity of the film on a homogeneous amine-ended substrate. (a) After spin-coating, before annealing. (b) After complete dewetting of the film.  $k_{z0}$  is the vertical component of the wavevector of the incident photons in a vacuum.<sup>[11]</sup>

Before dewetting, Kiessig fringes on the reflectograms testify for the presence of a continuous 14 nm thick film. After dewetting, the reflectogram only shows a broad Kiessig fringe originating from the silane monolayer in dry regions of the substrate. The regions covered by the droplets do not show up in the reflectogram, due to their high roughness and thickness. In agreement with XRR, AFM phase images show a very strong contrast between droplets and dry regions (Figure S3).

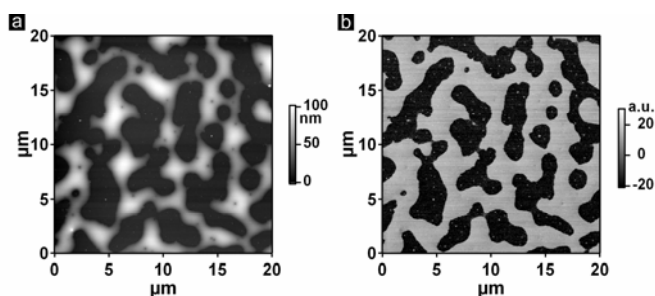


**Figure S3** IC-AFM images after complete dewetting of the BC film. (a) Topography image. (b) Phase image.

XPS spectra at grazing incidence (in order to have access to the outer most layer of the surface sample) also confirmed that dry holes are formed on the perfluorinated regions of nano-patterned surfaces at the end of the dewetting process. Since the borders of the dewetted trenches could shade the electrons in their way to the detector, the nano-patterns (lines) were aligned parallel to the source-detector direction. The results presented in Figure S4 indicate that fluorine can be detected by XPS in such conditions, which testifies for the dry nature of the fluorinated stripes after dewetting. A precise quantification is not possible since the sample, in the X-ray beam, is not homogeneous.

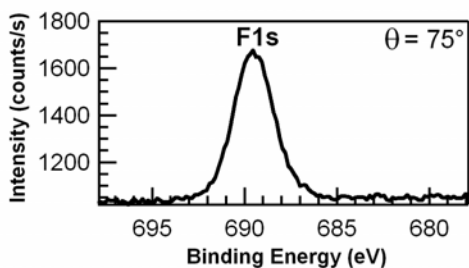


**Figure S4 XPS spectrum.** (F1s region) measured at grazing incidence, of a nano-patterned sample after dewetting.  $\theta$  is defined as the angle between the surface normal and the analyzer line of view.

## References

- 
- [1] C. J. van Oss, M. K. Chaudhury, R. J. Good, *Chem. Rev.* **1988**, *88*, 927.
  - [2] D. K. Owens, R. C. Wendt, *J. Appl. Polym. Sci.* **1969**, *13*, 1741.
  - [3] R. J. Good, in *Contact Angle, Wettability and Adhesion*, VSP, Utrecht, **1993**.
  - [4] W. H. Press, W. T. Vetterling, S. A. Teukolsky, B. P. Flannery, in *Numerical Recipes in C*, Cambridge University Press, Cambridge, **1992**.
  - [5] J. Brandrup, E. H. Immergut, in *Polymer Handbook*, Wiley, New York, **1989**.
  - [6] Y. Li, Y.-L. Loo, R. A. Register, P. F. Green, *Macromolecules* **2005**, *38*, 7745.
  - [7] J. Israelachvili, in *Intermolecular & Surface Forces*, Academic Press, New York, **1992**.
  - [8] M. S. Turner, M. Rubinstein, C. M. Marques, *Macromolecules* **1994**, *27*, 4986.
  - [9] C. Bollinne, S. Cuenot, B. Nysten, A. M. Jonas, *Eur. Phys. J. E* **2003**, *12*, 389.
  - [10] V. A. Parsegian, *Van der Waals Forces*, Cambridge University Press, New York, **2006**.
  - [11] A. Pallandre, K. Glinel, A. M. Jonas, B. Nysten, *Nano Lett.* **2004**, *4*, 365.